JOURNAL OF PROPULSION AND POWER
Vol. 18, No. 1, January–February 2002

# Design of a Fusion Propulsion System—Part 2: Numerical Simulation of Magnetic-Nozzle Flows

Ioannis G. Mikellides*
*Science Applications International Corporation, San Diego, California 92121*
Pavlos G. Mikellides†
*Ohio Aerospace Institute, Cleveland, Ohio 44142*
and
Peter J. Turchi‡ and Thomas M. York§
*The Ohio State University, Columbus, Ohio 43235*

**Numerical simulations of magnetic-nozzle flows have been successfully conducted in the interest of providing valuable insights and detailed design guidance to near-future experimental efforts. Quasi-steady modeling using helium propellant with classical resistivity demonstrates a nearly isentropic expansion of the confined gas to exhaust speeds that exceed 270 km/s. For a stagnation temperature of 100 eV, approximately 70% of the thermal power is converted to thrust power (0.4 GW), producing 4.6 kN of thrust. Further expansion can lead to additional gains in thrust by utilizing the thermal power that is retained in the 20-eV plasma at the exit. In the inlet of the nozzle, near the plasma field interface, the development of nonuniformities in the magnetic field is exposed. For $T_0 = 100$ eV as much as 50% of the mass flux is found to penetrate the current layer across the magnetic field lines. At fixed plasma pressure and applied field the layer at the throat increases in thickness from approximately 3 to 5 cm when the stagnation temperature is decreased from 250 to 100 eV.**

## Nomenclature

| | | |
|---|---|---|
| $A$ | = | cross-sectional area, m$^2$ |
| $B$ | = | magnetic field, T |
| $B_0$ | = | magnetic field at coil center, T |
| $\boldsymbol{b}$ | = | magnetic field unit vector |
| $J_B$ | = | magnet coil current, Amp |
| $L_B$ | = | magnet coil length, m |
| $\dot{m}$ | = | mass flow rate, kg/s |
| $N$ | = | magnet coil turns/length, m$^{-1}$ |
| $P$ | = | pressure, Pa |
| $P_0$ | = | stagnation pressure, Pa |
| $R$ | = | radius, m |
| $\Re$ | = | specific gas constant, m$^2$/s$^2$-°K |
| $T_0$ | = | stagnation temperature, °K |
| $u_\perp$ | = | velocity component perpendicular to magnetic field, m/s |
| $u_{\perp,\mathrm{res}}$ | = | resistive ("leaking") speed across the magnetic field, m/s |
| $\boldsymbol{V}$ | = | velocity vector, m/s |
| $W_0$ | = | power, W |
| $Z$ | = | charge state |
| $\alpha_\eta$ | = | electric diffusivity, m$^2$/s |
| $\gamma$ | = | ratio of specific heats |
| $\delta$ | = | current layer thickness, m |
| $\mu_0$ | = | permeability of free space, H/m |
| $\Psi$ | = | ratio of nozzle throat to coil radii |

Presented as Paper 2000-3367 at the AIAA/ASME/SAE/ASEE 36th Joint Propulsion Conference and Exhibit, Huntsville, AL, 16–19 July 2000; received 5 October 2000; revision received 15 July 2001; accepted for publication 20 July 2001. 

*Senior Staff Scientist, 9455 Towne Center Drive, Mail Stop W2076. Member AIAA.
†Senior Research Associate, 22800 Cedar Point Drive. Member AIAA.
‡Chief Scientist, Los Alamos National Laboratory, P.O. Box 1663, Mail Stop D410, Los Alamos, NM 87545. Associate Fellow AIAA.
§Professor, Department of Aerospace Engineering and Aviation, Aero/Astro Lab, 2300 West Case Road. Senior Member AIAA.

## Introduction

EXTENSIVE human exploration of the solar system requires propulsion systems that provide high thrust-to-weight (T/W) ratios for reduced travel times and high specific impulse values for increased payloads. For example, nearly straight trajectories would require exhaust speeds in the range of 200–500 km/s to achieve maximum payload fraction.[1] Thermonuclear fusion is the primary projected energy source that satisfies these requirements. Fusion reactants can be mixed with much higher mass flows of propellant gas to produce optimized exhaust speeds at the desired values of T/W. Critical features of fusion propulsion concepts can be evaluated using Godzilla,[2] a gigawatt-level facility with a 1.8-MJ pulseline. The facility can power a magnetoplasmadynamic (MPD) source[3] to provide plasma flow emulating that of a fusion-heated propellant. When stagnated within a magnetic cusp configuration, this flow will attain temperatures on the order of 100 eV. At such high temperatures the plasma requires properly shaped magnetic fields to guide the gas to high exhaust speeds through a "magnetic nozzle" while retaining sufficiently low cross-field mass loss and tolerable thermal loads to the surrounding walls. Proper operation of a magnetic nozzle in these high-energy-density propulsion systems requires current flow around the plasma. From a magnetohydrodynamic (MHD) fluid viewpoint current is generated by the pressure-gradient force acting across the confining applied field. Under idealized conditions interaction of this current with the magnetic field is just sufficient to stop the fluid motion across the field, leading to a state of magnetohydrostatic equilibrium. In dynamical systems operating with nonideal plasmas, a variety of convective and diffusive processes (classical and anomalous) will modify the gradients within the current layer and, under certain conditions, jeopardize its preservation. Both the thickness and downstream profile of the layer determine the extent to which supplied power is efficiently converted to thrust power. Accurate resolution of this plasma-field interface and quantitative accounts of power losses in a magnetic nozzle require numerical and experimental simulations.

## Preliminary Design

The Godzilla power source can provide 1 GW to a matched load at a maximum design charging voltage of 6 kV. The bank consists of 2100 capacitors (43 $\mu$F) that can discharge the maximum stored energy in a minimum pulse time of 1.625 ms. With a total transmission line impedance of 9 m$\Omega$, the maximum current to a matched load is $\frac{1}{3}$ MA. However, the bank configuration allows for relatively easy modification for variation of deliverable power, current level, and associated pulse time. Specifically, Godzilla is arranged in three racks comprising seven rows of capacitors in 10 sections of 10 capacitors each. This allows for each section to be connected in series to provide the maximum pulse time of 17 ms at a line impedance of 189 m$\Omega$. Electromagnetic acceleration of plasma propellant within an MPD configuration can provide exhaust speeds that correspond to stagnation temperatures of 100 eV (Ref. 3). Hydrogen propellant can be expanded through the main magnet coil to exhaust speeds in the excess of 200 km/s; however, the present experimental approach favors inert propellant (He) that can still provide the necessary insights at maximum speed of about 190 km/s. In this particular effort design of the main magnet coil will concentrate on the requirements of $T_0 = 100$ eV and $U_{ex} = 170$ km/s. Isentropic expansion of doubly ionized He ($\gamma = \frac{5}{3}$) implies exhaust temperatures $T_e = 20.12$ eV, Mach number $M_e = 3.45$, and radius ratio (throat-to-exhaust) of the converging-diverging magnetic nozzle $R_e/R_* = 2$. Design of the MPD plasma source[3] requires that the stagnation density is of the order of $\rho_0 = 5e{-}5$ kg/m$^3$ (stagnation pressure, $P_0 = 0.355$ MPa), which allows calculation of the mass flow rate per unit area at the throat $(\mathring{m}/A)_* = 3$ kg/m$^2$-s. This allows for the design of the throat radius based on power limitations

$$W_0 = \frac{(1+Z)\gamma \Re T_0}{\gamma - 1}\left(\frac{\dot{m}}{A}\right)_* \pi R_*^2 \tag{1}$$

where $\Re = 2075$ m$^2$/s$^2$-K and $Z = 2$. The power requirement is determined by first designing the magnet coil. The characterization of the magnetic nozzle's flow parameters allows this preliminary design. Based on the radius of the vacuum tank (30 cm), the magnet coil radius is reasonably chosen as $R_B = 20$ cm and the length is taken as $L_B = 32$ cm. For a finite length solenoid the field at the centerline and $L_B/2$ is given by

$$B_0 = \frac{L_B}{\sqrt{L_B^2 + 4R_B^2}}\mu_0 N J_B \equiv f_B \mu_0 N J_B \tag{2}$$

where $f_B = 0.625$ for the particular choice of radius and length of the solenoid. As a first-order approximation, we can equate the magnetic pressure before compression to the total stagnation pressure $B_0^2/2\mu_0 = P_0$, which yields a field of $0.944T$. Thus, from Eq. (2) and for $N = 100$ turns/length the magnet coil current $J_B = 12$ kA. At maximum charging voltage (6 kV) the input power required is 72.1 MW, which—by one possible configuration—can be delivered by redirecting one rack of capacitors with all 70 sections (10 capacitors each) in series. Specifically, the power output assuming a matched load at a line impedance of 189 m$\Omega$ is 95.6 MW, which meets the requirement, and thus the energy can be delivered in a pulse time of 5.6875 ms. This matched-load configuration requires that the last interstage inductance is equal to that of the solenoid, which can be achieved by iterating further on the combination of magnet current and turns/length.

The power requirement for the plasma flow then becomes $W_0 < \frac{2}{3}$ GW, which allows for a maximum throat radius of about 6 cm and exit radius of 12 cm at 0.617 GW. The associated ideal mass flow rate is then 34 g/s delivering thrust of 5.785 kN excluding any further potential expansion to vacuum pressure.

## Numerical Modeling

The interaction of several physical processes in the magnetic nozzle system that have intrinsically different scale sizes for time and distances, represents a major obstacle in the design of the experiment. Simplified theoretical modeling alone, using zero- and one-dimensional analyses,[4–6] is insufficient. It fails to provide the required detailed understanding on a variety of pertinent processes in the magnetic nozzle, such as resistive dissipation and turbulence, throughout their evolution. Large-scale computer simulation is therefore warranted in order to confirm the feasibility of the planned experiment (under the intended operating conditions) and to provide detailed coil specifications: magnetic field strength, geometry and position relative to the plasma source.

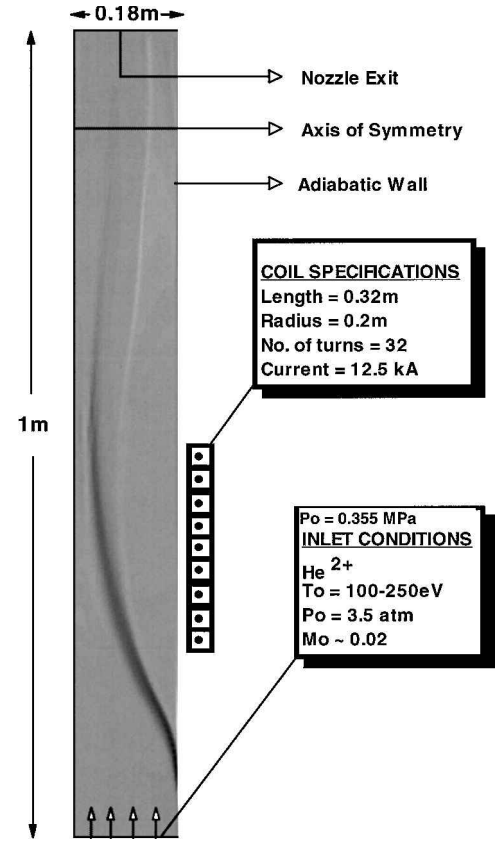


**Fig. 1 Magnetic nozzle geometry and specifications. The contour plot displays the simulated azimuthal current-density distribution $j_\theta$ at $t = 0.25$ ms and $T_0 = 100$ eV. Minimum value at half-point (throat) $\approx -5$ kA/cm$^2$. (The ensuing MACH2 plots are drawn with a larger aspect ratio (length/radius) for better clarity of contour and vector profiles.)**

Numerical simulation of the flowing plasma through a magnetic guide field (Fig. 1) was made possible by utilizing the time-dependent, two-and-one-half-dimensional, nonideal MHD code MACH2 (Ref. 7). The code solves the dynamic, single-fluid, resistive MHD equations in two dimensions while retaining all three spatial components of vector quantities. The computational mesh can be purely Eulerian, Lagrangian, or arbitrary. The latter feature was implemented in the present simulations in order to concentrate the grid in regions of sharp field gradients (Fig. 2). The simulated plasma flow consisted of fully doubly-ionized, helium plasma ($He^{2+}$). In addition to the conservation laws for mass and fluid momentum with the plasma pressure assumed isotropic, the energy equations for electrons and ions allowed for resistive heating while assuming thermal equilibrium between species. The thermal equilibration time for the lower temperature (100 eV) simulations was estimated to be approximately 10 times less than the characteristic plasma transit time through the nozzle. At the higher temperatures and lower densities the electron-ion equilibration times are more comparable to plasma transit times. Anisotropic effects on resistivity were computed based on the Braginskii formulas for transport coefficients. The evolution of the magnetic field during plasma transit through the nozzle was computed based on a magnetic induction equation that combines Maxwell's equations and the generalized Ohm's law. The present simulations did not include the effects of anomalous resistivity, Hall term, diamagnetic drift caused by electron pressure gradient nor thermoelectric contributions to the electric field.

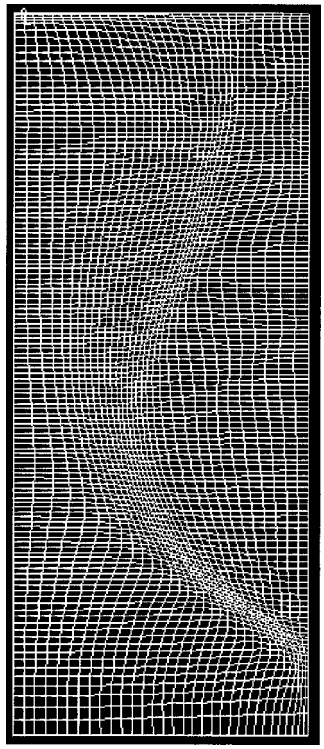

**Fig. 2 Adapted mesh arrangement (32 × 168) at $t$ = 0.24 ms.**

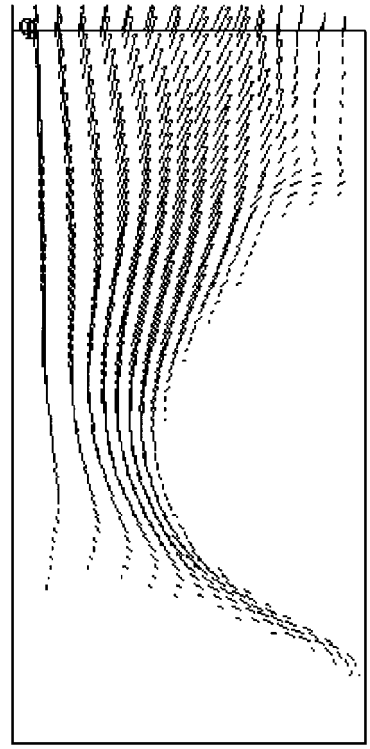

**Fig. 3 Velocity vectors ($T_0$ = 200 eV, $t$ = 0.24 ms).**

The simulated plasma flow initially entered a region of (vacuum) magnetic field applied by the external coil shown in Fig. 1. This initial solenoidal field distribution was calculated based on an algorithm[8] that incorporates the Biot–Savart law integrating individual current-carrying coil contributions. An adiabatic condition was imposed at the wall with plasma flow allowed to expand freely through the downstream, open-end boundary. At the centerline boundary, reflection symmetry was imposed. As implied by Fig. 1, the computational region simulates a 1-m-long cylindrical tube with a radius of 0.18 m.

## Core Plasma Flow

Earlier simulations with MACH2 confirmed the possibility of emulating the high-energy, fusion-heated plasma flow by means of a modified inverse-pinch switch (resembling an MPD thruster) on the Godzilla gigawatt-level pulser.[3] Under the available power levels the electromagnetic plasma source can provide high enough exhaust speeds to achieve the desired stagnation conditions. Specifically, the high-speed plasma is to be decelerated to nearly stagnation conditions of $T_0 \approx 100$ eV and $\rho_0 \approx 5e-5$ kg/m$^3$ through a magnetic cusp arrangement maintained by two magnet coils, and then accelerated again to supersonic speeds through a magnetic nozzle. The present work is a continuation of previous efforts to simulate the stagnated plasma through a magnetic guide field imposed by the main magnet coil.[9]

A series of simulations were performed to validate proper quasi-steady magnetic nozzle operation. Braginskii (classical) resistivity was assumed with the helium plasma treated as a constant-$\gamma$ gas (with $\gamma = \frac{5}{3}$). Simulations using a real equation of state, which is available in MACH2 (in tabular form) via the SESAME library, introduced no major differences when compared with the ideal-gas simulations. The three expected regions—core-plasma flow (Figs. 3 and 4), magnetic guide field (Fig. 5), and azimuthal-current layer (Fig. 1)—are distinctly identified. Under the aforementioned stagnation conditions the flow through the magnetic nozzle reached a quasi-steady state within approximately 0.1 ms (Fig. 6). The confined plasma expanded in a nearly isentropic fashion to a maximum exhaust Mach number of 3.4 with the sonic point located approximately halfway through the channel (Fig. 7). Table 1 compares MACH2-computed ratios of stagnation-to-throat and stagnation-to-exit conditions near the centerline with values calculated based on

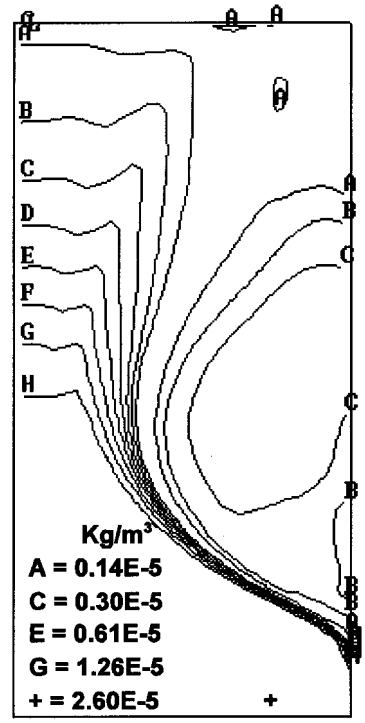


**Fig. 4 Mass density contours ($T_0$ = 200 eV, $t$ = 0.24 ms).**

the isentropic relations. The isentropic ratios at the exit were determined based on the exit Mach number that was computed by MACH2 near the centerline. Substantial exclusion of magnetic flux was achieved in the core plasma throughout the nozzle. At the location of the throat, less than 3% of the maximum field across the radius ($0.9T$) persisted within a distance of 2.5 cm from the axis of symmetry (Fig. 8).

A series of additional simulations at higher stagnation temperatures, but fixed applied field and stagnation pressure, captured the expected dependence of the (maximum) exhaust speed on the square root of the stagnation temperature (Fig. 9). The scaling indicates that the simulated magnetic nozzle is

**Table 1 Comparison between plasma flow through a magnetic nozzle from the MACH2 simulations (with values taken near the axis of symmetry) and isentropic flow of constant $\gamma$ (case: $T_0$ = 100 ev)**

| Location | Model | $\rho_0/\rho$ | $T_0/T$ | $P_0/P$ |
|---|---|---|---|---|
| Throat | Isentropic flow ($\gamma = \frac{5}{3}$) | 1.54 | 1.33 | 2.05 |
| | MACH2 | 1.55 | 1.36 | 2.10 |
| Exit | Isentropic flow ($\gamma = \frac{5}{3}$) | 10.1 | 4.67 | 47.2 |
| | MACH2 | 10.9 | 4.76 | 51.9 |

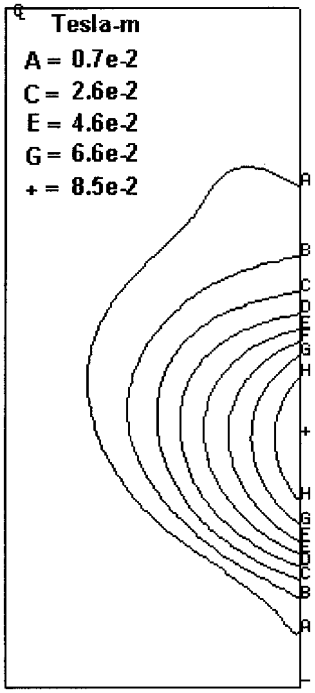


**Fig. 5 Magnetic field lines ($T_0$ = 100 eV, $t$ = 0.24 ms).**

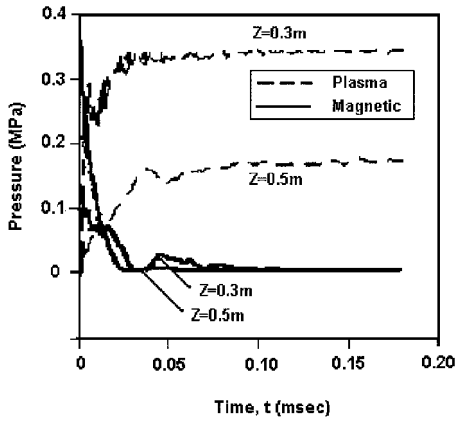


**Fig. 6 Evolution of plasma and magnetic pressures near the axis of symmetry at 30 and 50 cm from the inlet ($T_0$ = 100 eV).**

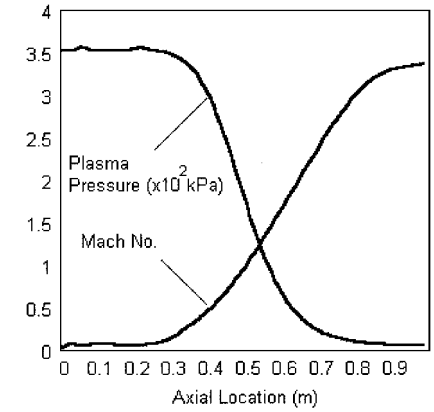


**Fig. 7 Pressure and Mach-number profiles along axis of symmetry for $T_0$ = 100 eV at $t$ = 0.24 ms.**

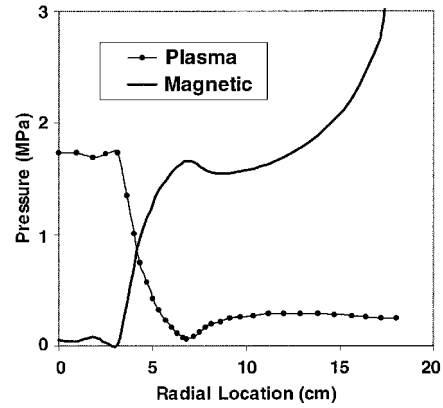


**Fig. 8 Radial profiles of plasma and magnetic pressures at the throat location ($T_0$ = 100 eV, $t$ = 0.24 ms).**

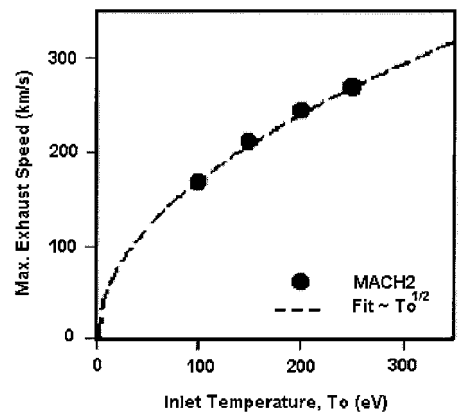


**Fig. 9 Maximum exhaust speed at different stagnation temperatures in steady state. Effective nozzle area ratio $Ae/A^* \sim$ 4.5.**

comparable to a solid, converging-diverging nozzle of an area ratio $A_e/A_* \sim 4.5$ and an average Mach number of 3.6. The simulations were largely conducted in the interest of gaining quantitative insight on mechanisms driving the formation of the current layer. The topic is discussed in greater detail in the following section.

## Current-Layer Formation

A critical issue in the magnetic nozzle is the manner in which plasma and field intermix during confinement. The spatial extent within which plasma and magnetic field interact is directly related to kinetic energy losses and cross-field mass transport. Furthermore, the interface is subject to variety of potentially destructive MHD and microinstabilities that can develop during plasma transit through the nozzle.

Our ability by means of numerical simulation to investigate properly the formation of the layer depends largely upon the inherent limitations of a two-dimensional, axisymmetric, MHD code such as MACH2. Physical processes that possess fine-scale features such finite Larmor-radius effects are beyond the realm of validity of an MHD simulation. Moreover, trapped-particle instabilities and anomalous transport must rely upon phenomenological models (derived from kinetic theory principles) to determine their potential implications.

Even within the validity of resistive MHD, a number of pertinent unstable modes with possibly destructive consequences on magnetic nozzle operation have an inherent three-dimensional nature and are

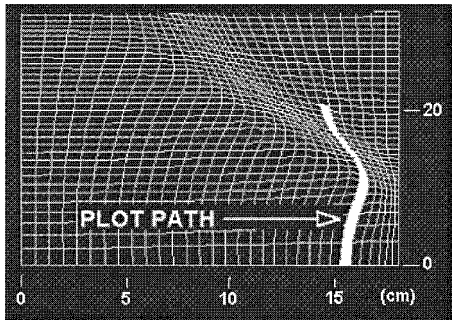


**Fig. 10 Half-section of the computational region (32 × 128 mesh) with highlighted plotting path.**

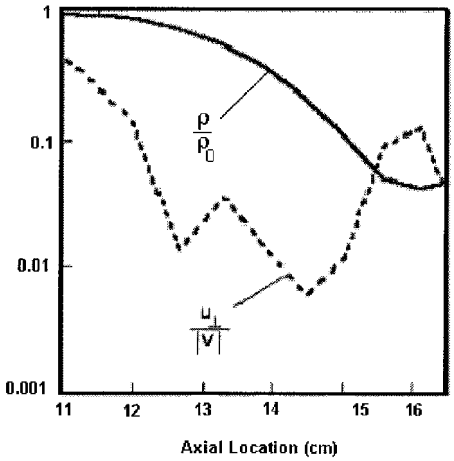


**Fig. 11 Axial variation of density ratio and fractional speed across the current layer near the nozzle inlet (along the highlighted path of Fig. 10).**

best studied with a three-dimensional MHD code. For example, gravitational (or otherwise "g-mode") instabilities that can be driven by "bad" magnetic curvature in the nozzle entrance and exit, as well as Kelvin–Helmholtz instabilities (driven by ExB shear), all have wave vectors in the azimuthal direction and act in a manner that distorts axisymmetry.

With the preceding restrictions in mind we turn to the results of the present numerical simulations, specifically as they relate to the formation of the current layer along the nozzle. With the fluid speed normal to the magnetic field determined by,

$$|u_\perp| = \sqrt{|\boldsymbol{V}|^2 - (\boldsymbol{V}\cdot\boldsymbol{b})^2} \tag{3}$$

the axial variation of $u_\perp/|\boldsymbol{V}|$ at the inlet demonstrates that almost 50% of the mass flux infiltrates the layer (Figs. 10 and 11). Equivalently, for a process during which plasma and field (under force balance) interact by way of resistive diffusion the leaking speed across the field can be approximated by,

$$|u_{\perp,\mathrm{res}}| = \frac{\alpha_\eta}{B^2/\mu_0}\nabla_\perp P \approx \frac{\alpha_\eta}{B^2/\mu_0}\frac{P}{\delta} \tag{4}$$

For resistive interaction between plasma and field near the inlet, Eq. (4) gives approximately 0.17 km/s for the cross-field speed. The value determined by MACH2 using Eq. (3) is roughly 4.5 times higher (0.75 km/s). By way of comparison, Eqs. (3) and (4) give 0.108 and 0.098 km/s, respectively, for conditions at the throat validating the scaling assumed by Eq. (4). The extent of numerical contribution ("artificial diffusion") to the mass penetration was found to be minimal after simulations with a finer grid were performed. Specifically, a 64 × 128-node mesh resulted in an almost identical localization of the adapted grid (in steady state), resulting simply in a finer resolution of the current layer (Fig. 12). A comparison of plasma and magnetic pressure profiles across the layer, near the

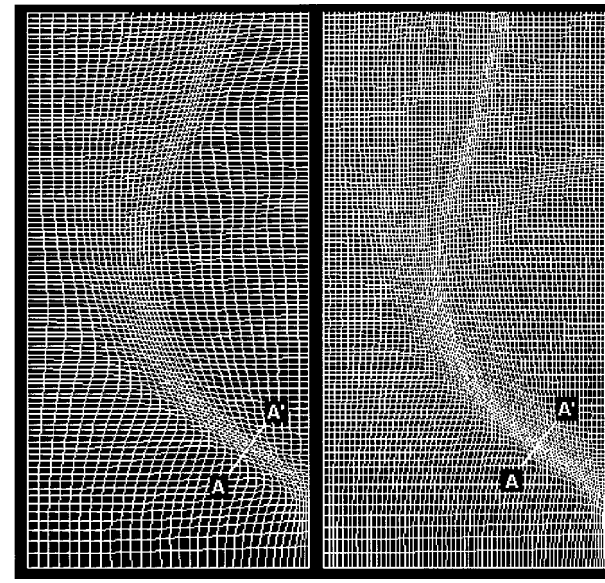


**Fig. 12 Comparison of adapted grid arrangements: left, 32 × 128 mesh; right, 64 × 128 mesh.**

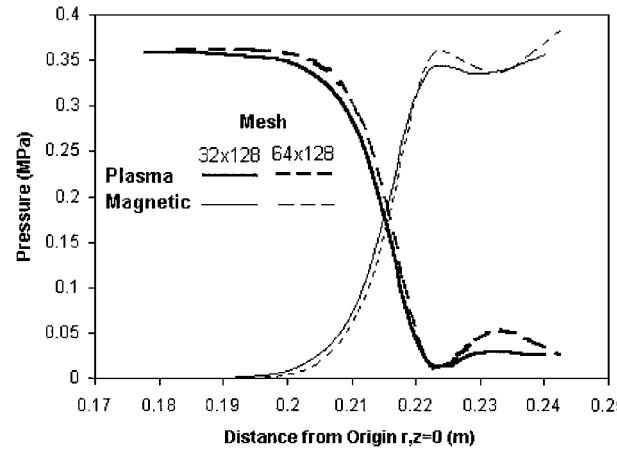


**Fig. 13 Comparison of plasma and magnetic pressures using two different grid arrangements: 32 × 128 and 64 × 128 nodes. Profiles are plotted across paths $A-A'$ (see Fig. 12).**

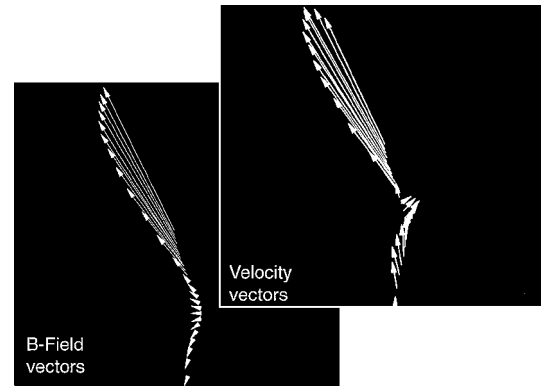


**Fig. 14 Axial variation of velocity and magnetic field vectors along the highlighted path of Fig. 10.**

stagnation region, revealed little difference between the two cases (Fig. 13). The almost identical characteristic layer thickness computed with the different mesh configurations implies that the determining mechanism for the observed mass loading of the layer is independent of the grid choice (as long as a sufficient number of nodes is provided to resolve the gradients in the region).

Figure 14 suggests that the penetration at the inlet is allowed by a tendency of the field lines to break away from the direction of

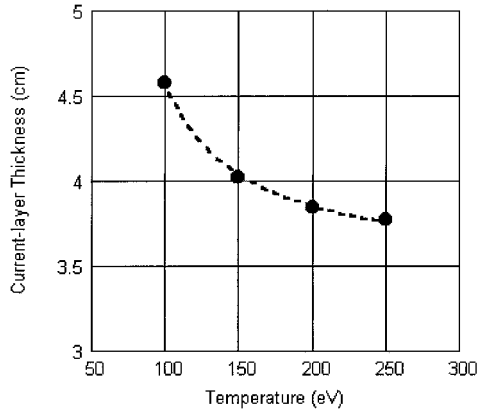


**Fig. 15 Variation of current-layer thickness with stagnation temperature as computed by MACH2 at the throat.**

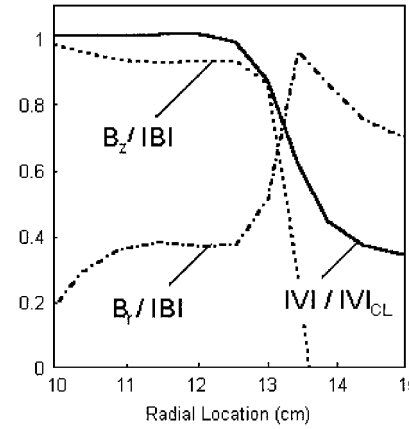


**Fig. 16 Profiles of flow speed (in reference to value at the axis of symmetry) and magnetic field (unit vector) components at the nozzle exit.**

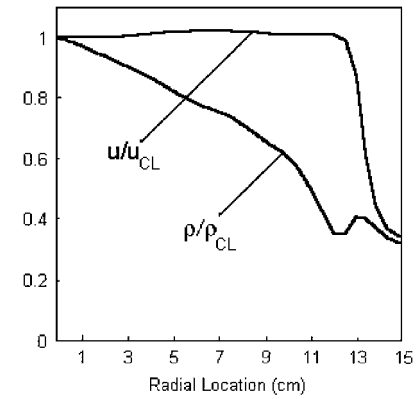


**Fig. 17 Profiles of density and axial velocity at the nozzle exit (in reference to conditions at the axis of symmetry).**

the flow. The behavior is akin to changes in the topology of the field observed in fusion devices such as field-reversed theta pinches (FRTPs) during magnetic reconnection. In contrast to FRTPs however, where the reconnection rate depends not only on resistivity but also on the reverse bias field trapped during implosion,[10,11] the activity in the magnetic nozzle depends largely on the ability of the dynamic pressure to oppose field-line reversion. The tendency for reconnection is further enhanced at the nozzle inlet by the condition of axial flow along the wall boundary. The cusped field configuration can therefore alleviate the effect once the secondary magnet coil is added, by allowing fluid streamlines and field lines to adjust more freely under conditions of low resistivity.

The penetrating mass flux serves as a pumping mechanism during the formation of the current layer. Under the relatively slow spatial variation of plasma conditions near the inlet, the quasi-steady extent of the layer in the region depends largely upon the rate at which flow of mass into the layer is expelled from regions of high flux penetration. At the higher stagnation temperatures and lower densities the speed ratio $u_\perp/|\boldsymbol{V}|$ near the inlet increases, but the total mass flux decreases allowing for less mass into the layer. Upon entering the layer, the flow of plasma remains strongly coupled to the field. Near the throat, and further downstream, cross-field transport is mainly a result of resistive diffusion ($u_\perp \approx u_{\perp,\mathrm{res}}$) with opposing plasma inertia and field curvature forces becoming increasingly important in the evolution of the layer to its quasi-equilibrium extent. Figure 15 portrays the variation of the layer thickness at the throat as calculated by MACH2 for various stagnation temperatures but fixed stagnation pressure and applied field. Closer to the nozzle exit further dispersion of the layer combines with high radial diversion of the magnetic field lines to induce reductions in ideal nozzle performance.

## Exhaust Flow and Propulsive Performance

The manner in which the plasma expands downstream of the throat has important repercussions on the performance of the nozzle. Integrated conditions across the exit (for the case of $T_0 = 100$ eV) indicate that the magnetic nozzle produces approximately 4.6 kN (1025 lbf) of thrust at a (maximum) exhaust speed of 170 km/s (Figs. 3 and 9 ). Referring to Fig. 8, for a throat radius of 7.2 cm and stagnation conditions $P_0 = 0.355$ MPa and $T_0 = 100$ eV the corresponding mass flow rate based on isentropic flow through a converging–diverging nozzle is 50 g/s. At this rate, and assuming uniform conditions across the exit, the ideal thrust would be almost 45% higher at approximately 8.4 kN (1890 lbf).

Downstream of the throat the plasma has gained sufficient axial momentum, while retaining a high magnetic Reynolds number (>1000), to induce a bell-shaped contour pattern (e.g., see Figs. 3 and 5). Although the effect is favorable as it reduces radial losses of axial momentum ($u_r < 0.15u_z$ at the exit), the strong coupling between plasma and field introduces additional losses to the highly conducting exhaust. These losses are evident in Fig. 16. Between 12–14 cm the flow speed (plotted in reference to conditions at the axis of symmetry) is reduced by approximately 60%. The magnetic field profile implies a region of high radial diversion of the lines as they make their way back to the coil. Consequently, the relatively hot (20 eV) plasma experiences a resistive drag force[12] during its motion across the field. The reduction of directed axial momentum in this annular section is therefore not caused by radial diversion of the fluid streamlines (commonly associated with flow expanding from conical solid nozzles) but by a reduction in total flow speed by the resistive drag force as the particles detach from the magnetic field lines.[6] Approximately one-half of the reduction in the ideal thrust (24%) takes place between 12–14 cm.

Closer to the axis of symmetry, the axial velocity is seen to follow a uniform profile along the exit for approximately $\frac{2}{3}$ of the channel radius. The density is (smoothly) reduced by 65% from its value at the axis of symmetry (Fig. 17). The reduction is caused by the sustained interaction between plasma pressure and magnetic field in the region. The associated azimuthal currents are relatively low in magnitude but extend to a larger radius because of the continued broadening of the layer downstream of the throat. With the exclusion of parallel (to $\boldsymbol{B}$) electron thermal conduction (no thermal-diffusive effects were included in the present simulations), the plasma temperature follows a relatively gradual drop across the exit as allowed by the negligible rates of resistive heating that occur in the exhaust. Possible expansion of the flow to uniform-density conditions would imply an estimated 21% increase in thrust without accounting for any additional reductions caused by resistive drag further downstream. These reductions may be enhanced if electron thermal conduction allowed for substantial heat transfer from the hot upstream plasma to the exhaust. For the simulations at $T_0 = 100$ eV the characteristic timescale for heat transfer by means of parallel electron thermal conduction $\sim L^2/a_{\mathrm{ke}}$ (with $L$ being the nozzle length and $a_{\mathrm{ke}}$ being the parallel electron thermal diffusivity in square meters/second) is found to be approximately two times higher than the characteristic time for axial plasma transit through the nozzle $\sim L/V$ (based

on conditions at the nozzle throat). At the higher temperatures and lower densities the effect is expected to introduce more significant deviations from the isentropic result. Nonclassical electron thermal conduction can also be important, as shown by previous studies,[13] and would therefore further alter deductions that are based on ideal mechanisms alone.

Beyond the 15-cm point low-density plasma exits the channel at a rate of approximately 3 g/s (total mass flow rate at exit is 30 g/s). The flow of plasma here is caused by accumulated cross-field mass losses along the nozzle. These occur mainly from the outer segment of the layer at the inlet (see Fig. 11) and near the exit as plasma escapes the main axial outflow to follow the radially diverging magnetic field lines (~1 g/s). The former (responsible for approximately 1 g/s) is caused by the interaction of the layer with the wall boundary and can therefore be mitigated upon utilization of the cusped-field arrangement. As illustrated in Fig. 8, the plasma that has escaped the core flow has sufficient pressure to cause modest modifications to the magnetic field distribution in the region. Based on the simulated mass flow rate of 30 g/s, approximately 70% of the thermal power is converted to thrust power (0.4 GW). The high-temperature plasma at the exit is found to retain more than 0.1 GW into its thermal modes, implying that additional conversion of thermal to thrust power is possible.

## Conclusions

Critical features of magnetic-nozzle flows have been quantitatively investigated by utilizing the two-dimensional simulation tool MACH2 as a resistive-MHD code. The code's adaptive-grid capabilities allowed for the accurate resolution of the steep gradients that persist in the expected thin current layer throughout its evolution along the nozzle. During quasi-steady transit of the resistive plasma flow through the injection region (inlet), nonuniformities in the magnetic field led to substantial penetration of mass flux into the current layer. Cross-field mass loss is observed near the exit as plasma escapes the main axial outflow to follow the radially diverging magnetic field lines. Detachment of plasma in this region results in a 24% reduction of the ideal thrust. Additional mass loss is allowed by the interaction of the layer with the wall boundary, near the inlet, and can therefore be alleviated upon utilization of the cusped magnetic field configuration as originally perceived for the total acceleration system. Conditions at the exit indicate that additional conversion of thermal to thrust power is possible.

## Acknowledgments

The continued support and encouragement for this effort by Craig Williams, NASA John H. Glenn Research Center, Cleveland, Ohio, is gratefully acknowledged. The authors also benefitted from conversations with Richard Gerwin of the Los Alamos National Laboratory, Los Alamos, New Mexico. This work was supported by NASA John H. Glenn Research Center and by the Ohio Supercomputer Center, Columbus, Ohio.

## References

[1] Williams, C. H., and Borowski, S. K., "An Assessment of Fusion Space Propulsion Concepts and Desired Operating Parameters for Fast Solar System Travel," AIAA Paper 97-3074, July 1997.

[2] Turchi, P. J., Gessini, P., and Mikellides, P. G., "Gigawatt, Quasi-Steady Plasma Flow Facility for Fusion Rocket Simulations," AIAA Paper 98-3592, July 1998.

[3] Turchi, P. J., and Mikellides, P. G., "Theoretical Design of Gigawatt-Level MPD Plasma Source for Studies of Magnetic-Nozzle Confinement in Fusion Propulsion Systems," *26th International Electric Propulsion Conference*, IEPC Paper 99-013, Oct. 1999.

[4] Sercel, J. C., "A Simple Model of Plasma Acceleration in a Magnetic Nozzle," AIAA Paper 90-2597, July 1990.

[5] Chubb, D. L., "Fully Ionized Quasi One-Dimensional Magnetic Nozzle Flow," *AIAA Journal*, Vol. 10, No. 2, 1972, pp. 113, 114.

[6] Hooper, E. B., "Plasma Detachment from a Magnetic Nozzle," *Journal of Propulsion and Power*, Vol. 9, No. 5, 1993, pp. 757–763.

[7] Peterkin, R. E., Jr., and Frese, M. H., "MACH: A Reference Manual—First Edition," U.S. Air Force Research Lab., Phillips Research Site, Kirtland, New Mexico, July 1990.

[8] Mikellides, P. G., "A Theoretical Investigation of Magnetoplasmadynamic Thrusters," Ph.D. Dissertation, Dept. of Aeronautical and Astronautical Engineering, Ohio State Univ., Columbus, OH. 1994.

[9] Turchi, P. J., Mikellides, P. G., and Gessini, P., "Numerical Simulation of Magnetic Nozzle Flow for Nuclear Fusion Space Propulsion," AIAA Paper 99-2701, June 1999.

[10] Milroy, R. D., and Brackbill, J. U., "Numerical Studies of Field-Reversed Theta-Pinch Plasma," *Physics of Fluids*, Vol. 25, No. 5, 1982, pp. 775–783.

[11] Pietrzyk, Z. A., "Numerical Simulation of Field-Reversed $\theta$-Pinches," *Journal of Applied Physics*, Vol. 52, No. 1, 1981, pp. 183–186.

[12] Gerwin, R. A., Marklin, G. J., Sgro, A. G., and Glasser, A., "Characterization of Plasma Flow Through Magnetic Nozzles," Los Alamos National Lab., Los Alamos, New Maxico, AL-TR-89-092, Final Rept., Feb. 1990.

[13] York, T. M., Jacoby, B. A., and Mikellides, P. G., "Plasma Flow Processes Within Magnetic Nozzle Configurations," *Journal of Propulsion and Power*, Vol. 8, No. 5, 1992, pp. 1023–1030.